11-1-2007

NGC 5548: THE AGN ENERGY BUDGET PROBLEM AND THE GEOMETRY OF THE BROAD-LINE REGION AND TORUS

C. Martin Gaskell
University of Nebraska-Lincoln, mgaskell@ucsc.edu

Elizabeth S. Klimek
University of Nebraska-Lincoln, eklimek@nmsu.edu

Ludmila S. Nazarova
Euro Asian Astronomical Society, Universitetskij Pr. 13, Moscow 119899, Russia

Submitted to Astrophysical Journal
Preprint typeset using LaTeX style emulateapj v. 03/07/07

NGC 5548: THE AGN ENERGY BUDGET PROBLEM AND THE GEOMETRY OF THE BROAD-LINE REGION AND TORUS

C. MARTIN GASKELL[1] AND ELIZABETH S. KLIMEK[2]
Department of Physics & Astronomy, University of Nebraska, Lincoln, NE 68588-0111

AND

LUDMILA S. NAZAROVA[3,4]
Euro Asian Astronomical Society, Universitetskij Pr. 13, Moscow 119899, Russia

Submitted to Astrophysical Journal

ABSTRACT

We consider in detail the spectral energy distribution (SED) and multi-wavelength variability of NGC 5548. Comparison with the SEDs of other AGNs implies that the internal reddening of NGC 5548 is E(B-V) = 0.17 mag. The extinction curve is consistent with the mean curve of other AGNs found by Gaskell & Benker, but inconsistent with an SMC-type reddening curve. Because most IR emission originates exterior to the broad-line region (BLR), the SED seen by the inner BLR is different from that seen by the outer BLR and from the earth. The most likely BLR covering factor is $\sim 40\%$ and it is not possible to get an overall BLR covering factor of less than 20%. This requires that the BLR is not spherically symmetric and that we are viewing through a hole. Line-continuum variability transfer functions are consistent with this geometry. The covering factor and geometry imply that near the equatorial plane the BLR covering approaches 100%. The spectrum seen by the outer regions of the BLR and by the torus is thus modified by the absorption in the inner BLR. This shielding solves the problem of observed BLR ionization stratification being much greater than implied by photoionization models. The BLR obscuration also removes the problem of the torus covering factor being greater than the BLR covering factor, and gives consistency with the observed fraction of obscured AGNs. The flux reduction at the torus also reduces the problem of AGN dust-reverberation lags giving sizes smaller than the dust-sublimation radii.

Subject headings: galaxies:active — galaxies:quasars:general — X-rays:galaxies — black hole physics — accretion: accretion disk — dust, extinction

1. INTRODUCTION

Because of the difficulty of observing in the extreme ultra-violet (EUV), the true shape of the continuum of AGNs has long been a mystery. If emission lines arise from photoionization, then the equivalent width of the lines gives information on the number of ionizing photons (Zanstra 1931, Osterbrock 1989) and their total energy (Stoy 1933). Early photoionization model calculations of the broad-line region (BLR) spectrum (e.g., Davidson 1972, MacAlpine 1972, Shields 1972) *assumed* covering factors ($\Omega/4\pi$) and continuum shapes that could account for the observed strengths of the emission lines. However, the first spectrophotometry of the rest-frame UV continuum in high-redshift AGNs showed an apparent turn down of the UV spectrum (Oke 1970, 1974). *IUE* satellite observations of lower-redshift AGNs confirmed this (Green et al. 1980). Green et al. reported that the $\alpha \approx 0.5$ spectral slope ($F_\nu \propto \nu^{-\alpha}$) from the optical to the UV steepened to $\alpha \approx 2.3$ at wavelengths shorter than λ1200. MacAlpine (1981) showed that there was a severe "energy budget" problem because such a continuum needed $\Omega/4\pi \gtrsim 9$ to match the observed He II λ4686 equivalent width. The observed ionizing continuum was thus providing an order-of-magnitude fewer ionizing photons than were needed.

The problem was compounded when spectroscopy of the Lyman-limit region showed that rest-frame Lyman continuum absorption was rare (Osmer 1979). Smith et al. (1981) concluded from observations of the Lyman-limit region that $\Omega/4\pi \lesssim 0.15$ and further analysis by MacAlpine (1981) showed that $\Omega/4\pi \approx 0.05$ was most likely. Netzer (1985) pointed out that there is a serious energy-budget discrepancy for other lines. The HST composite spectrum of Zheng et al. (1997) and the multi-wavelength spectra of a sample of PG quasars (Laor 1997) confirmed the steepening of the observed continuum at shorter wavelengths. Photoionization models (e.g., Shields & Ferland 1993; Korista et al. 1998; Goad & Koratkar 1998; Kaspi & Netzer 1999; Korista & Goad 2000) consistently required covering factors an order of magnitude higher than allowed by the limits on Lyman limit absorption.

An important question is whether the continuum *we* see is the same as that seen by the emission lines. The continuum could be intrinsically anisotropic, or the continuum we see could be modified by extinction from dust grains along the line of sight, or by absorption lines. MacAlpine (1981) suggested that a marked upturn in dust extinction below λ1200 could be causing the apparent turndown in the continuum we see.

Green et al. (1980), however, felt that the turndown

[1] Present Address: Department of Astronomy, University of Texas, Austin, TX 78712-0259. Electronic address: gaskell@astro.as.utexas.edu
[2] Present Address: Department of Astronomy, New Mexico State University, Las Cruces, NM 88003-0001. Electronic address: eklimek@nmsu.edu
[3] Electronic address: lsn@kzn.ru
[4] Visiting scientist, Department of Physics and Astronomy, University of Nebraska

below λ1200 was probably intrinsic, and that extinction by dust grains was probably not causing it because of the lack of effect on the spectrum longwards of λ1200. McKee & Petrosian (1974) had previously argued against the presence of dust in AGNs because of the lack of both the λ2175 dust feature and the curvature in the UV spectra that dust should produce. The apparent match up between UV spectral indices and the X-ray region (Laor 1997) argued against significant extinction.

Various other solutions have been offered to the energy-budget problem. Collin-Souffrin (1986), Joly (1987), and Dumont, Collin-Souffrin, & Nazarova (1998) favored non-radiative heating of the BLR as the solution to the energy-balance problem. Binette et al. (1993) suggested the clouds were being heated by a diffuse continuum very close to them. Korista, Ferland, & Baldwin (1997) suggested the the UV-EUV SED might be double peaked. Maiolino et al. (2001c), on the other hand, suggested that the solution to the conflict between the lack of Lyman limit absorption and the high covering factors implied by photoionization models was that the BLR was not covering the source uniformly.

In this paper we investigate the energy-budget question in the well-studied AGN NGC 5548 and investigate the implications for the BLR and torus structure. NGC 5548 is an important test case for investigating the energy-budget issue (Rokaki et al. 1994; Dumont et al. 1998) since NGC 5548 has been particularly well studied at all accessible wavelengths, its variability behavior in most spectral regions is well known, and the line-continuum transfer functions, which give information on the BLR size and radial distribution, are better known than for any other AGN. We focus in this paper on the period 2449115 – 2449130 when NGC 5548 was intensely monitored by the *Hubble Space Telescope*. We adopt a distance, R, of 76 Mpc to NGC 5548. This is based on an $H_0 = 73$ km/s/Mpc, $\Omega_{matter} = 0.27$, $\Omega_{vacuum} = 0.73$ cosmology and the local velocity field model of Mould et al. (2000).

2. THE SPECTRAL ENERGY DISTRIBUTION OF NGC 5548

Many different spectral energy distributions (SEDs) have been considered when modelling NGC 5548. A number of these SEDs are illustrated in Fig. 2 of Dumont et al. (1998), in Chiang & Blaes (2003), and Fig. 1 of Steenbrugge et al. (2005). It can be seen that the SEDs differ by up to factors of three in the region below the Lyman limit and elsewhere. We therefore start off by reconstructing the probable SED of NGC 5548 around JD 2449120 in detail.

Like all AGNs, NGC 5548 varies. It was in fact the very first AGN for which variability was discovered (see historical discussion in Gaskell & Klimek 2003). This variability has to be allowed for in constructing the continuum shape. As far as possible, one needs simultaneous observations of the continuum at different wavelengths. However, such observations are not available for all wavelength regions, so, where there were no simultaneous observations, we have estimated the fluxes by scaling observations from other epochs. For determining the appropriate scalings we have used other sets of quasi-simultaneous data. These scalings are necessary for estimating the SED at a given epoch, but they should also be useful for modeling spectral variability at different epochs.

TABLE 1
Observed and Corrected Continuum Fluxes

Region	Log(ν)	Log(νF_ν)[a]	MW de-red	Internal de-red
100 μm	12.48	-10.14		
60 μm	12.70	-10.29		
25 μm	13.08	-10.00		
12 μm	13.40	-10.03		
10.2 μm	13.46	-10.15		
5 μm	13.80	-10.32		
3.4 μm	13.93	-10.08		
2.2 μm	14.13	-10.10		
1.65 μm	14.27	-10.03		
1.25 μm	14.38	-10.06		
5200 Å	14.76	-10.24	-10.21	-10.13
4820 Å	14.79	-10.25	-10.22	-10.10
4650 Å	14.81	-10.27	-10.23	-10.10
2250 Å	15.12	-10.29	-10.20	-9.72
2050 Å	15.17	-10.29	-10.20	-9.69
1820 Å	15.22	-10.24	-10.17	-9.63
1490 Å	15.30	-10.24	-10.16	-9.59
1360 Å	15.34	-10.21	-10.13	-9.54
1179 Å	15.41	-10.23	-10.12	-9.53

[a] νF_ν in ergs s^{-1} cm^{-2}

From the 73-day period JD 2449061 to 2449134 NGC 5548 was simultaneously monitored with the *Hubble Space Telescope*, the *IUE* satellite, and many optical observatories (Korista et al. 1995). From the period of *HST* coverage we have selected JD 2449115 - 2449130 when NGC 5548 was in a high state. During this period data were available only for some of the optical and UV continua and emission lines, so in the following subsections we describe, in order of construction, how the continuum in each waveband was obtained.

2.1. *Optical and UV*

In Table 1 we give our measured optical continua from the *International AGN Watch (IAW)* optical spectra (see Wanders & Peterson 1996[5]). Three relatively line-free sections of the spectra between major emission lines were taken to represent the continuum. These sections were defined by the observed wavelength ranges: 4640–4660 Å, 4810–4830 Å, and 5190–5210 Å. We measured average UV continuum points from the HST spectra (Korista et al. 1995) during the high state at $\lambda\lambda$ 1170, 1360, 1490, 1820. 2050, and 2250 Å. We used observed wavelength ranges of 1160–180 Å, 1344–1374 Å, 1478-1501 Å, 1804-1834 Å, 2022-2204 Å, and 2225-2241 Å.

To obtain fluxes in other passbands, when there were no simultaneous observations, we scaled observations to our optical or UV fluxes. There are many broad-band optical photometric observations available but these include host-galaxy contamination. We need to correct for different host galaxy contributions and differing passbands. The *IAW* database gives monochromatic fluxes at 5100Å standardized to a 5×7.6 arcsecond spectroscopic aperture. Romanishin et al. (1995) discuss how to estimate the nuclear flux of NGC 5548 from direct images and they give the transformation between the

[5] Note that all the line and continuum fluxes in their paper are too low by a factor of two.

5100Å fluxes and V-band fluxes. They give estimates of AGN-free galaxy magnitudes as a function of photometric aperture and give the host galaxy light contribution to the standard IAW spectroscopic aperture. They estimate the galaxy flux in the standard photometric aperture to be 2.53×10^{-15} ergs s^{-1} cm^{-2} Å^{-1}, while the galaxy contribution in an 8-arcsecond radius photometric aperture is 5.81×10^{-15} ergs s^{-1} cm^{-2} Å^{-1}.

Although for our modeling below we consider the host-galaxy-free AGN optical fluxes, for comparison with other wavelengths, our observed fluxes (column 2 of Table 1) still include the galaxy contribution since this is included by other observers. In section 4 we subtract host galaxy contributions from all wavebands.

2.2. *Infra-red*

Even though infra-red radiation is not relevant in providing ionizing photons, it does contribute to the heating of the broad line region and hence to the total energy budget. As we will discuss below (see section 2.3), in order to know the IR flux received by the BLR clouds one needs to know the distance of the IR emitting regions from the center. It will also be important to know the inner radius of the dusty torus because, as proposed by Netzer & Laor (1993) and Laor (2007), we will find that this is probably the outer edge of the BLR.

To our knowledge, there were no simultaneous infrared observations made at the time of the HST observations. We can, however, estimate the IR flux from the relationship between the IR and optical at other times. From a study of 41 Seyfert galaxies, Glass (2004) reported that all but two showed variability, with K-band (2.2 μm) amplitudes in the range < 0.1 to > 1.1 mag. The shortest timescale he found for detectable changes was one week. Glass found that, in general, the near-IR flux varies in the same way as the optical, UV, and X-ray flux, but with a time delay. For NGC 5548 he reports observations in the J, H, K, & L bands made on 12 nights over the three-year period 1988 - 1990. Lyutyi & Doroshenko (1993) give UBV photometry during the same period.

The delay of the IR fluxes relative to the optical and UV is substantial so the IR flux depends on the optical flux at an earlier time. Furthermore there will be an additional delay in IR radiation from the dust getting back to the BLR clouds. The lag of the IR flux was not measured for NGC 5548 in the high state we consider, but we can estimate the lag by scaling from the measurements of the lag by Suganuma et al. (2004) when NGC 5548 was in a low state and independently by scaling from other objects.

Glass (2004) gives estimated delays and 3.4μm luminosities for 17 AGNs. In Fig. 1 we show the relationship between the IR lag, τ, and luminosity. A least squares fit gives

$$\log(\tau) = 0.48\log(L_{3.4\mu m}) - 9.14 \qquad (1)$$

This correlation is completely consistent with the expected $\tau \propto L^{0.5}$ relationship for a constant dust sublimation temperature. Minezaki et al. (2005) and Suganuma et al. (2006) find a similar correlation between τ and the V-band absolute magnitude. For NGC 5548, $L_{3.4\mu m} = 22.81$, so Fig. 1 implies a delay of ~ 84 days.

Suganuma et al. (2004) monitored NGC 5548 in the IR and optical bands from JD 2451950 to JD 2452825, when NGC 5548 was in a low state. They measured time delays between the K band and the V band of 48 ± 3d and 47 ± 6d. Even though the mean V-band flux of NGC 5548 decreased by a factor of about 2.8 between the earlier epoch we are considering, their lags can be used to check our estimate if we consider the change in the level of activity. Due to dust sublimation, an increase in luminosity leads to an increase in the effective torus radius, thereby increasing the lag between the IR and the optical according to the relationship $\tau \propto \sqrt{L}$ (Oknyanskij et al. 1999.) Thus, when the measured lag is scaled by the ratio of the average luminosities during the two epochs, we should get a lag consistent with our estimate. Scaling of the Sugnuma et al. lag gives 79 d, which is in good agreement with our earlier estimate of 84 d from the general IR radius–luminosity relationship, and within the error bars of the Suganuma et al. lags.

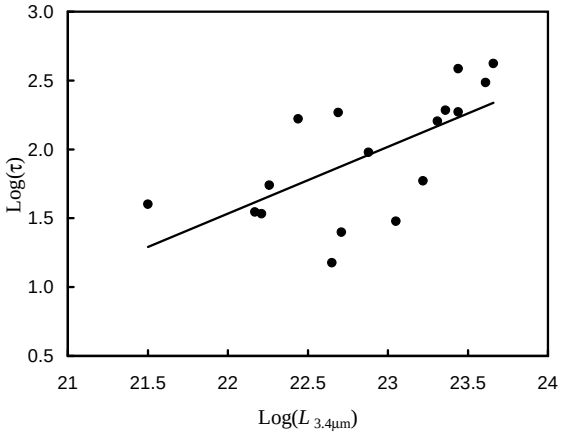

FIG. 1.— IR lags, τ (in days), as a function of L-band flux (log WHz^{-1}) for 17 AGNs. The lags are the responsivity-weighted lags of the J and L band fluxes relative to the U band fluxes. The line is a least-square fit. Data from Glass (2004).

By comparing the J-band (1.25 μm) fluxes of Glass (2004) with the average V magnitudes 80 days earlier, from Lyutyi & Doroshenko (1993) we get the approximate relationship:

$$J = 0.4V + 6.2 \qquad (2)$$

To estimate the IR continuum seen *by the BLR* from the optical continuum we need to look at the optical continuum, not at a time τ earlier, but at a time $\sim 2\tau$ earlier. This is because the UV/optical continuum heating the dust takes $\sim \tau$ days to get to the dust torus, and the reprossed IR takes *another* $\sim \tau$ days on average to get back to the BLR. Because of the larger size of the IR-emitting region, we took the average optical flux (from Korista et al. 1995) between $2\tau - 50$ days before and $2\tau + 50$ days before our high and low states. After appropriate scaling of the Korista et al. fluxes to the magnitudes of Lyutyi & Doroshenko (1993), we obtained J magnitudes of 11.63 and 11.66 for our high and low states. As would be expected, the IR flux does not follow the more rapid UV/optical changes.

Choloniewski (1981) showed that, in the optical, the shape of the *variable* component of AGNs remains the same as the flux level changes (see also Winkler et al. 1992). The analysis of Glass (2004) shows that, for any given AGN, the colors of the variable component of the

IR emission are also usually independent of the level of activity and, for his whole sample, he finds that the colors of the variable components fall within moderately narrow ranges. We have therefore used our calculated J magnitude and the average IR colors of Glass to get estimated H, K, and L magnitudes of 10.77, 10.05, and 8.76 respectively for the low state, and 10.74, 10.02, and 8.73 for the high state. These fluxes fall well within the historical ranges of fluxes given in the literature.

For longer IR wavelengths we have taken measurements from the literature. Potential problems with these measurements include inhomogeneity due to varying data quality and photometric apertures used, and source variability. We excluded measurements that were taken using apertures larger than 15" diameter, as these measurements contain significant additional off-nuclear infrared emission from the host galaxy. For the M (4.8 μm) waveband we averaged the fluxes of McAlary, McLaren, & Crabtree (1979) and McAlary et al. (1983), and for the N (10 μm) waveband we averaged the fluxes of Kleinmann & Low (1970), Rieke & Low (1972), and Rieke (1978). There is observational evidence that for these longer IR wavelengths non-simultaneity is not a problem. Neugebauer et al. (1989) found that while AGNs show variability in J, H, K, and L, there was no variability at 10 μm. Similarly, Edelson & Malkan (1987) found that there was no evidence for variability in the *IRAS* passbands for non-blazar AGNs.

The 12, 25, 60, and 100 μm IRAS observations (Moshir et al. 1990) have a low spatial resolution and no variability information is available. They refer to a region much further out in the galaxy than the near-IR torus.

2.3. *IR Continuum Seen by the BLR*

A large fraction of the IR continuum in an AGN is clearly not coming from the central source, but from a torus well outside the BLR. The ratio of IR to optical/UV that a distant observer sees is *not* the same as what a BLR cloud sees.

Calculating the X-ray, UV, and optical flux at the BLR clouds is straight forward. We assume that the region emitting this flux is smaller than the BLR and located inside it. We can then obtain the flux by simply multiplying the flux observed at the earth by $(R/r)^2$ where $R = 9.05 \times 10^{10}$ ld is the distance to NGC 5548, and r is the distance of the BLR clouds from the center. For the IR, for which a substantial part of the emission observed from the earth arises from emission from the torus *outside* the BLR, the assumption of a compact source within the BLR is incorrect, and we will overestimate the flux at the BLR if we just scale the flux in the same way as the X-ray, UV, and optical. Instead, the IR flux at the BLR clouds depends on the surface brightness of the IR emitting regions and the solid angles they subtend.

We roughly estimated the relative dilution of the IR continuum at the BLR clouds with the following scheme. We divided the radiation received by a BLR cloud at radius r_c into two components: the radiation originating from $r < r_c$ and the radiation originating from $r \geq r_c$. We assumed that the flux of radiation originating at $r < r_c$ could be scaled from the flux received at the earth by $(R/r)^2$, where R is the distance to NGC 5548. If we consider a uniform thin spherical emitting shell of radius r_{shell}, the radiation density falls off as r^{-2} for $r > r_{shell}$ while it is constant for $r \leq r_{shell}$ (i.e., within the shell). This still remains a reasonable approximation if the emitting matter is in a ring rather than a shell. Therefore, for radiation originating outside r_c the flux was scaled by $(R/r_{shell})^2$. Thus the IR radiation contribution from outside the BLR was reduced by $(r_c/R_{shell})^2$ relative to the contribution from inside the BLR.

To estimate the fraction of IR radiation from within r_c we assumed there was a minimum accretion-disk temperature of 5000 K. Any IR flux less than that produced by the spectrum of a 5000 K black body was assumed to come from outside r_c and reduced by $(r_c/Rshell)^2$. In a standard thin accretion disk (Pringle & Rees 1972, Shakura & Sunyaev 1973) the temperature, T falls off with radius as $r^{-0.75}$. If there is reprocessing of radiation from the inner regions to the outer regions then the temperature gradient is shallower (e.g., $T \propto R^{-0.50}$ for the "slim disk" of Abramowicz et al. 1988). If dust is in thermal equilibrium with radiation from a compact source, $T_{dust} \propto R^{-0.50}$ as well, so we assume that $T \propto R^{-0.50}$. This implies that the effective radius emitting a given wavelength is $R_{eff} \propto \lambda^2$. The reduction of the IR radiation is thus $\propto \lambda^4$. The contribution from outside the BLR can thus be ignored at all but the shortest wavelengths.

Because of this effect, BLR clouds at different radii receive different long-wavelength SEDs. The outer BLR is close to the inner edge of the torus and experiences a K-band flux similar to that given by a simple inverse-square-law scaling; the inner BLR is an order of magnitude closer and receives 100 times less relative K-band flux from the dust than would be expected by simple scaling. In our photoionization modeling we therefore use different SEDs at different radii.

2.4. *Hard X-rays*

2.4.1. *Relationship Between Hard X-ray and Optical/UV Flux Levels*

There were no simultaneous hard X-ray observations during the HST campaign, so we need to estimate the hard X-ray flux from the optical and UV. Uttley et al. (2003) show that the 2–10 keV flux measured with *RXTE* is well correlated on *long* timescales (months) with the optical flux at λ5100. However, on short timescales (day-to-day), the X-rays in NGC 5548 can vary a lot while the optical varies little (see Uttley et al. 2003 and Gaskell et al. in preparation). We compared the RXTE 2–10 keV fluxes from Uttley et al. (2003) with the 5100Å fluxes (from the *IAW* database) measured within $\pm$7 d. The median separation time between the X-ray and optical observations is 0.6 d. As can be seen in Fig. 2, there is a direct proportionality, after subtracting the galaxy contribution as estimated by Romanishin et al. (1995). We found that, apart from short-term events on the timescale of a month or two, the average X-ray/optical ratio was constant in time and showed no correlation with the optical flux level. The X-ray flux, in units of 10^{-11} ergs s^{-1} cm^{-2}, can be predicted from the optical by the equation

$$F_{2-10keV} = 0.564 \times F_{\lambda 5100}, \quad (3)$$

where the $F_{\lambda 5100}$ is in units of 10^{-15} ergs s^{-1} cm^{-2} Å^{-1}.

Clavel et al. (1992) (see their Fig. 4) found that the 2–10 keV flux observed with *Ginga*, was also directly

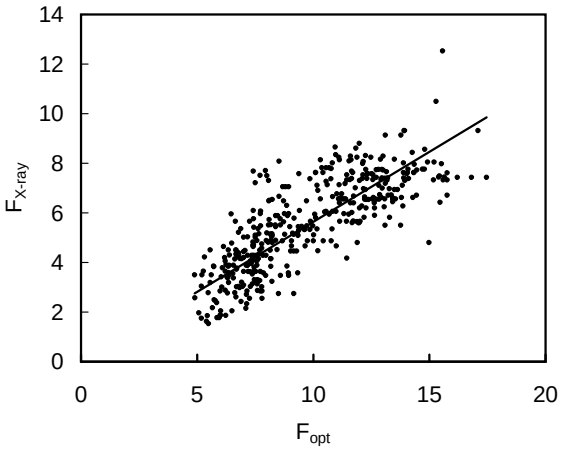

FIG. 2.— The relationship between the 2–10keV flux (in units of 10^{-11} ergs s^{-1} cm^{-2}) and the host-galaxy subtracted optical flux (in units of 10^{-15} ergs s^{-1} cm^{-2} Å^{-1}) for near simultaneous observations. The straight line is the relationship $F_{2-10keV} = 0.564 \times F_{\lambda 5100}$

proportional to the 1350Å flux:

$$F_{2-10keV} = 0.114 \times F_{\lambda 1350}. \quad (4)$$

In our high state, $F_{\lambda 5100} = 6.49 \times 10^{-15}$ after host-galaxy subtraction, and $F_{\lambda 1350} = 44.8 \times 10^{-15}$. From equations (3) and (4) these predict $F_{2-10keV} = 3.7 \times 10^{-11}$ and 5.1×10^{-11} ergs s^{-1} cm^{-2} respectively. We adopt a mean of 4.4×10^{-11} ergs s^{-1} cm^{-2}.

2.4.2. *Shape of the Hard X-ray Spectrum*

As in most AGNs, the shape of the hard X-ray spectrum of NGC 5548 can be described by a power law ($F_\nu \propto \nu^{-\alpha}$) with a spectral index $\alpha \sim 0.7$. In NGC 5548 α depends on the flux level. Markowitz, Edelson, & Vaughan (2003) show, from *RXTE* data, that for NGC 5548 the degree of hard X-ray variability is constant as a function of energy on short timescales but decreases for higher energies on long timescales. Chiang et al. (2000) and Papadakis et al. (2002) find a good correlation between α and $F_{2-10keV}$. From Fig. 4 of Chiang et al. and our estimated $F_{2-10keV}$ fluxes we get $\alpha = 0.76$. This is within the range found by Magdziarz et al. (1998) and also consistent with the trend found by Walter & Courvoisier (1990).

The hard cut-off in the γ-ray region is well constrained by *OSSE* spectra from the *Compton Gamma Ray Observatory*. Magdziarz et al. (1998) get a hard energy cutoff of 120 keV for 1991 and 1993 *OSSE* observations.

2.5. *Extreme Ultraviolet and Soft X-ray Region*

The most energetically important region of the spectrum of AGNs is the extreme ultraviolet (EUV) and soft X-ray spectral region. This is also the region responsible for most of the ionization of the BLR. Unfortunately, it is very hard to observe AGNs in the EUV and soft X-ray spectral region because of heavy atomic absorption.

Walter et al. (1994) present *ROSAT* soft X-ray observations of several AGNs, including NGC 5548. For all objects they find a strong soft X-ray excess above the extrapolation of the higher energy X-rays to lower energies. They find that the soft X-ray spectral shape is very similar in the different sources even though they range over four orders of magnitude in luminosity. The soft X-ray excess can be described by a bump with a similar cutoff energy of $kT \sim 200$ keV for sources with a wide range of luminosity. For NGC 5548 itself, the effective temperature of the soft excess appears to remain constant at $kT \sim 400$ eV (see Fig. 7b of Magdziarz et al. 1998). More recent *XMM-Newton* and *Beppo-SAX* observations (Pounds et al. 2003) also show a clear soft excess below 700 eV which, after allowance for complex absorption, probably smoothly extends to 2 keV in agreement with the Walter et al. (1994) spectrum. There is debate over whether the derived temperature of the soft excess in AGNs is real, or whether the apparent exponential cutoff is due instead to strong relativistically smearing of a partially-ionized absorption (Gierlinski & Done 2004), but the fundamental nature of the soft excess does not affect the continuum the broad-line region sees, so long as the BLR sees the same continuum we see.

There was no simultaneous monitoring of the soft X-ray spectrum during the *HST/IUE* campaign. We must therefore try to estimate the EUV/soft-X-ray flux from either the UV or the hard X-ray components. To do this we need to consider the nature of EUV variability and the relationship of EUV and soft X-ray variability to variability of the continuum at higher and lower energies.

2.5.1. *Variability of the Soft Component*

Our knowledge of variability of the EUV/soft X-ray flux of NGC 5548 has come primarily from monitoring with the *ROSAT* satellite, covering 0.1 – 2.4 keV, and the *EUVE* satellite, giving effectively measurements at a single energy of ~ 0.2 keV. Walter & Courvoisier (1990) found that as NGC 5548 varied, although the ratio of the soft excess to the higher energy power law component changed, the shape of the *soft* X-ray spectrum did not. *EUVE* count rates cannot be readily converted into flux units because the conversion depends on the spectral shape and hydrogen column density (see Marshall et al. 1995), but given the apparent constancy in the spectral shape, they are important for showing the *relative* variability at ~ 0.2 keV.

Observations reveal two important things about the soft excess. The first is that *the soft excess varies most.* The ratio of changes in the hard and soft X-ray components during the *ROSAT* monitoring of Nandra et al. (1993) is consistent with the soft excess varying more, and the *ROSAT* monitoring of Done et al. (1995) shows that variability is primarily at energies of less than 0.4 keV (see their Fig. 2). From subsequent simultaneous *EUVE* and X-ray monitoring of NGC 5548, Chiang et al. (2000) found that the amplitude of the *EUVE* variability was 15 – 20% greater than that of the *RXTE* variability.

The second important thing is that, on short timescales, *the soft excess leads the variability.* Kaastra & Barr (1987) discovered from *EXOSAT* monitoring of NGC 5548 that the soft X-rays led the hard X-rays by about 1.5 hours. Walter & Courvoisier (1990) found a similar leading of about 1 hour. Chiang et al. (2000) found that the EUV (0.2 keV) led the 0.5–1 keV ASCA band in NGC 5548 by 0.15 ± 0.05d, and led the RXTE 2–20 keV band by 0.45 ± 0.11d. These small delays are unimportant for our analysis, but the sign of the delay together with the greater amplitude of variability of the soft excess implies that *short-term X-ray variability is*

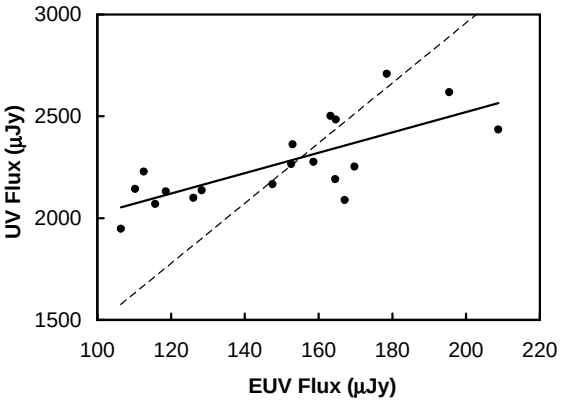

FIG. 3.— UV fluxes at 1350Å, observed with the *IUE* satellite versus *EUVE* 84Å fluxes (from Marshall et al. 1997) averaged over ±1d. The solid line is a least-squares fit. The dashed line represents a constant ratio of EUV to UV flux.

driven by variability of the soft excess. The width at zero intensity of the EUV/hard X-ray cross correlation function of Chiang et al. (2000) is ±1d. The size of the EUV emitting region is thus $\lesssim 1$ lt.d. The *EUVE* light curve of Chiang et al. (2000) shows there are sometimes changes of up to a factor of two on a timescale of an hour. We can thus be confident that the EUV to soft X-ray emission originates well inside the BLR.

2.5.2. *Correlation of Soft Excess with Lower Energies*

Although there were no simultaneous soft X-ray spectral measurements during the 1993 *HST* campaign, Marshall et al. (1997) made *EUVE* observations which overlap some of the UV observations, and despite the problem of converting *EUVE* counts to fluxes, the *amplitude* of EUV/soft X-ray variability can be estimated from the *EUVE* observations since the *EUVE* samples part of the *ROSAT* band at ~ 0.2 keV. This monitoring is important for showing the *relative* change in the flux of the soft excess as a function of the UV flux.

The *EUVE* observations over the period JD 2409104 – 2409112 (shortly after the high state we are considering) overlap the *HST* monitoring, and other *EUVE* observations overlap the *IUE* monitoring. The amplitude of the EUV variability is about ~ 5 times greater than the UV variability at λ1350. The EUV light curve shows continual variations of a factor of ~ 2 on timescales of one or two days. The later *EUVE* light curve of Chiang et al. (2000) shows similar variations. For the most prominent event seen both in the EUV and UV spectra, Marshall et al. find a lag consistent with zero delay between the two bands.

In Fig. 3 we show the correlation between the *EUVE* fluxes reported by Marshall et al. and the λ1350 UV flux measured by the *IUE* and *HST*. We have averaged *EUVE* fluxes within ±1d of the UV flux measurement. From a least-squares fit we find that

$$f_{EUV} = 0.11 f_{1350} - 97. \quad (5)$$

The range of EUV variability during the Marshall et al. (1997) monitoring was a factor of two, while the UV range was only a factor of 40%. Equation (5) and Fig. 3 imply that there is another component of UV flux that will remain even when the EUV flux goes to zero, at least on the timescale of the Marshall et al. observations.

Support for a correlation of the EUV with longer wavelengths is also provided by Dietrich et al. (2001), who made optical observations simultaneous with the Chiang et al. (2000) EUV and hard X-ray observations. Over the 30-day monitoring period, the optical and EUV fluxes are correlated (see Fig. 4 of Dietrich et al.), but the EUV flux varied by a factor of $\gtrsim 6$ while the observed optical flux variations were only 20%. Dietrich et al. find optical-EUV lags consistent with zero, but with fairly large errors of $\pm$ 2 – 3^d.

We used the UV flux rather than the optical flux to estimate the what the observed EUV/soft X-ray flux would have been during the period we are considering because the difference in amplitude between the UV and EUV is not as great as between the optical and the EUV, and because the UV is closer to the EUV in $\log(\nu)$ than the optical is, and thus the UV has a higher probability of being physically connected to the EUV. The estimated observed EUV flux is not the true EUV flux because of the atomic absorption (see Steenbrugge et al. 2005 and references therein). We can get a better estimate of the true EUV and soft X-ray flux by scaling to the higher energy side of this region, since the absorption problems are less. We therefore used the Walter et al. (1994) soft X-ray spectral shape relative to the comparatively absorption-free harder X-ray flux, which has been estimated above.

2.5.3. *Relationship Between the Soft and Hard X-ray Components*

The relationship between the soft and hard X-ray components provides an additional consistency check on our estimate of the soft component. As noted above, the hard X-ray variations lag the variations of the soft excess by a fraction of a day. From simultaneous *ASCA* and *EUVE* monitoring in 1996, Haba et al. (2003) found that, from day to day, the EUV and 2–10 keV X-ray fluxes were well correlated. The EUVE amplitude over a 10-day period was only 40% greater than the hard X-ray amplitude. As noted already, the 1998 simultaneous ASCA and EUVE monitoring by Chiang et al. (2000) showed a good correlation between the EUV and 2–10 keV X-ray fluxes, with the EUV amplitude being only 15 – 20% greater than the X-rays. Haba et al. did find, however, that on a shorter timescale (6 hours), there was a strong 40% dip in the EUV that had no counterpart in the hard X-rays (see their Fig. 2), but such rapid variability is not relevant for the emission lines we study here.

Walter & Courvoisier (1990) fit the lowest energy observed with the thin Lexan filter on *EXOSAT* with a power law extrapolated from the hard X-rays and a soft-component. The soft-excess generally makes up 90% of the flux in the filter. In Fig. 4 we show the relationship between the soft-excess and the hard X-ray component. There is a similar relationship between the hard X-rays and the soft excess as between the UV and the soft excess (see Fig. 3). Given that the 2–10 keV flux is correlated with the optical and UV on the BLR light-crossing timescale (see section 2.4), the amount of EUV variability implied by the relationship between the hard and soft X-ray fluxes is similar to that implied by the optical and UV.

3. THE GALACTIC REDDENING CORRECTION

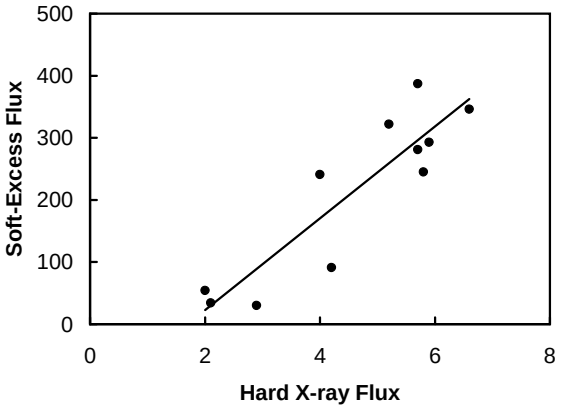

FIG. 4.— Soft Excess (in counts) vs. Hard X-ray component (in units of 10^{-11} ergs s^{-1} cm^{-2})

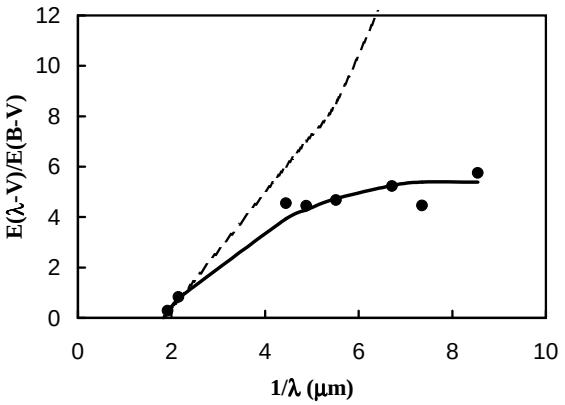

FIG. 5.— The extinction curve for NGC 5548 (filled circles) compared with the mean AGN reddening curve of Gaskell & Benker (2007) (solid curve) and an SMC reddening curve (dashed line).

The observed continuum fluxes must first be corrected for Galactic extinction. Schlegel et al. (1998) used measurements of dust emission at 100 and 240 μm to create Galactic extinction maps, which have an accuracy of 16%. From these the extinction, E(B-V), is 0.020 ± 0.003 mag for the direction of NGC 5548. From 21-cm observations Murphy et al. (1996) have determined the neutral hydrogen column density, n_H, towards NGC 5548 to be 1.62×10^{20}. If we adopt a standard dust-to-gas ratio of $E(B-V) = 1.72 \times 10^{-22} n_H$ (Bohlin, Savage & Drake 1978), we get E(B-V) = 0.028. If adopt a minimal dust-to-gas ratio of $E(B-V) = 1.2 \times 10^{-22} n_H$ (see Fig. 1 of Congiu et al. 2005) we get E(B-V) = 0.020. We can thus be confident that the Galactic reddening is relatively low and we adopt $E(B-V) = 0.024 \pm 0.004$

The Galactic extinction curve is well-determined for the near-IR, optical, and UV. For the far and extreme UV and soft X-ray regions the shape of the extinction curve is not observationally determined so we used the interstellar dust model of Draine (2003b) for $R = A_V/E(B-V) = 3.1$, which is a good fit to longer wavelengths (Draine 2003a).

4. HOST GALAXY CORRECTION

The observed spectral energy distribution we have compiled is not the spectral energy distribution of the AGN alone: emission from the host galaxy is also included. Schmitt et al. (1997) have made a compilation of spectral energy distributions for normal galaxies, which enables us to subtract off the host galaxy contributions at various wavelengths. Romanishin et al. (1995) find that the galaxy component of NGC 5548 is a normal early-type spiral, with no conclusive evidence of star formation in the bulge. We have therefore adopted the spiral galaxy SED of Schmitt et al. (1997). We scaled the spiral galaxy SED to a flux at 5200 Å of 3.6×10^{-15} ergs s^{-1} cm^{-2} Å^{-1} $= 3.3 \times 10^{-26}$ ergs s^{-1} cm^{-2} Hz^{-1} in the standard spectroscopic aperture of the *IAW*.

5. INTERNAL REDDENING CORRECTION

Gaskell & Benker (2007) have obtained extinction curves for individual AGNs by assuming that the unreddened continua are the same. For most of the AGNs they consider this gives extinction curves which resemble the reddening curve in the local solar neighborhood minus the λ2175 amorphous carbon feature, but which are flatter in the UV (see also Czerny et al. 2004 and Gaskell et al. 2004). For one of the AGNs they consider they find a steeply-rising, SMC-type reddening curve. We obtained the extinction curve for NGC 5548 in the same manner as Gaskell & Benker by comparing our observed spectrum of NGC 5548 with the observed blue spectrum of the relatively unreddened AGN 3C 273. As can be seen in Fig. 5, the resulting reddening curve is consistent with the mean AGN reddening curve of Gaskell & Benker (2007) but is inconsistent with an SMC reddening curve. Because of the consistency with the standard AGN reddening curve we have adopted the latter for NGC 5548. The normalization of NGC 5548 to the standard AGN curve gives $E(B-V) = 0.17$ mag. This has a formal uncertainty of $\sim \pm 0.01$ mag., but the real uncertainty is probably several times this because of the uncertainty in the host galaxy correction for 3C 273.

If we assume the standard Galactic dust-to-gas ratio of Bohlin et al. (1978) within NGC 5548, E(B-V) = 0.17 corresponds to a total hydrogen column of 10^{21} cm^{-2}. This is the same as the median column density Walter & Courvoisier (1990) obtain. Steenbrugge et al. (2005) get total best-fit column densities for their warm absorber components of 3×10^{21} cm^{-2} which would imply E(B-V) ~ 0.5 with a standard gas/dust ratio but this is not necessarily inconsistent with our lower reddening since not all warm-absorber gas will have dust associated with it.

The Gaskell & Benker (2007) reddening curve only extends to Lyman α. They find that the slope of AGN spectra in the far UV ($\lambda <$ Ly α) is not well correlated with E(B-V) determined from UV-optical spectra (see their Fig. 7) and they propose that the scatter in the far-UV slope is the result of a small amount of additional reddening (E(B-V) ~ 0.03 mag.) by a SMC-like dust since this spectral region is very sensitive to such dust. The bluest AGNs have a spectral index from $\sim$ 1200Å to $\sim$ 800Å of ~ 0.75. We have adopted this as the unreddened spectra slope in this spectral region.

The mean AGN extinction curve is uncertain at high energies. We therefore extrapolated the extinction curve to the X-ray region using the average of the Milky Way R = 3.1 and R = 5.5 curves calculated by B. Draine. These is based on the carbonaceous - silicate dust model of Weingartner & Draine (2001) and Li & Draine (2001). The graphite and silicate optical properties are given in Draine (2003a,b), and include structure around X-ray

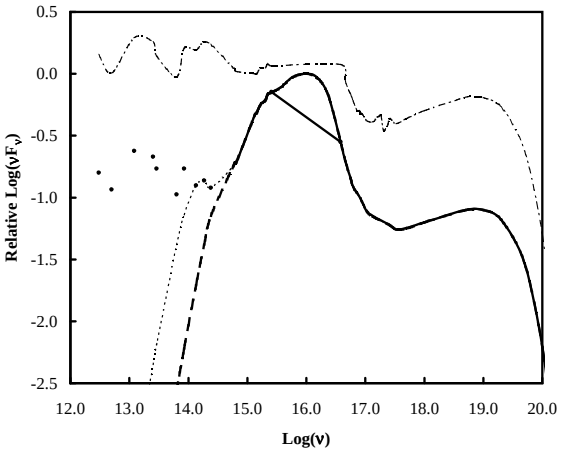

FIG. 6.— Estimated spectral energy distribution of NGC 5548 around JD 2449120. The upper dashed line represents the raw observed or estimated continuum before any reddening or host galaxy corrections. The thick solid line and the dots show the corrected observed continuum from the optical to the X-ray region including the interpolations in the EUV gap. This represents the SED as it would be seen from the earth with no extinction and no host galaxy light. The straight line shows the gap. The IR observations are shown as dots, while the lower dashed lines show the IR at 7 ld (thick dashed) and at 80 ld (thin dashed). The vertical scale is arbitrary.

TABLE 2
DE-REDDENED CONTINUUM FLUXES

Log(ν)	Log(νF_ν)[a]	Log(ν)	Log(νF_ν)[a]
12.5	-10.19	16.5	-9.79
13.0	-10.07	17.0	-10.47
13.5	-10.17	17.5	-10.63
14.0	-10.20	18.0	-10.81
14.5	-10.25	18.5	-10.51
15.0	-9.87	19.0	-10.52
15.5	-9.51	19.5	-10.74
16.0	-9.38	20.0	-11.79

[a] νFν in ergs s^{-1} cm^{-2} at the earth

absorption edges.

6. ADOPTED SPECTRUM

The only remaining uncertainty in our derived spectrum (see Fig. 6) is the "EUV gap". After our reddening corrections the νFν spectrum is rising on either side of the gap. We interpolated across the gap by fitting a 6th-order polynomial to the points on either side of the gap. This gives a good fit on either side of the gap and we consider this to be the most likely interpolation through the gap. We also did a simple linear interpolation across the gap and this is also shown in Fig. 6. The latter is most unlikely to be the correct interpolation, but this extreme case shows the maximum uncertainties introduced by our extrapolation. For convenience we also tabulate our final continuum in Table 2. This gives the continuum as it would be seen from the earth with no extinction and no host galaxy light contamination.

7. EMISSION-LINE FLUXES

In Table 3 we give the observed emission-line fluxes for the highest state during the period we consider. The

TABLE 3
EMISSION-LINE FLUXES

Line		Obsd.	MW de-red	Int. de-red
Lyα	λ1216	480	600	2300
N V	λ1240	93	120	450
O I	λ1304	30	40	140
O IV] + Si IV	λ1400	90	110	430
C IV	λ1549	730	870	3200
He II	λ1640	75	89	320
C III]	λ1909	135	160	550
Mg II	λ2798	130	150	400
He II	λ4686	15	16	30
Hβ	λ4861	62	70	120
He I	λ5876	11	12	18
Hα	λ6563	250	270	390

Ly α, C IV, and CIII] fluxes are from Korista et al. (1995), the Hβ flux is from Wanders & Peterson (1996)[6], and the He II λ1640 flux is from Bottorff et al. (2002). As Bottorff et al. discuss, there is a large uncertainty ($\sim$ 30%) in this flux. There are also even larger uncertainties in measuring He II λ4686 (see Appendix in Bottorff et al. 2002) and, in addition, the He II λ4686 line was not measured in the 1993 campaign. The value given in Table 1 was scaled from the 1989 campaign results. Hα was also not observed in the 1993 campaign so the strength given in Table 1 comes from assuming that Hα/H$\beta \approx 4.1$ (Shapavalova et al. 2004). The slight variations in this ratio with time (see Shapavalov et al.) are unimportant for our analysis. He I λ 5876 was also not observed during the 1993 campaign, so in Table 3 we have simply scaled it from Hβ using the median He I λ5876/Hβ ratio from Osterbrock (1977). As can be seen from Shapavalova et al. (2004) He I λ5876 varies substantially. Table 3 also gives the fluxes corrected for Galactic and internal reddening as discussed above.

8. REDDENING FROM LINES

Emission-line ratios can potentially give an independent check on reddening derived from the continuum. The He II recombination lines give the most intrinsically reliable line ratios, since they are mostly independent of physical conditions, but, as has been extensively discussed by Bottorff et al. (2002), measuring the He II λ1640/λ6886 ratio is very difficult (see their Appendix), so while the He II fluxes in Table 3 are consistent with the adopted reddening, the He II line ratio does not provide a reliable constraint.

The Balmer decrement is sensitive to physical conditions and varies both with projected velocity (see Snedden & Gaskell 2004, 2007a,b) and with time, but the relative integrated Hα/Hβ ratio is an approximate indicator of reddening (e.g., De Zotti & Gaskell 1985). Shapavalova et al. (2004) find Hα/Hβ varying from 3.5 to 4.3, which is not too different from Osterbrock (1977). If we adopt an unreddened decrement of 3.0, then the NGC 5548 decrements give E(B-V) $\sim$ 0.17 – 0.36, both which are consistent with the reddening we get from the continuum.

9. PHOTOIONIZATION MODELLING

[6] See Footnote 1

After determination of the continuum we ran models using the photoionization code CLOUDY, version 96.01 (Ferland et al. 1998) to determine the emission-line spectrum. In order to match the source-to-cloud distances found from reverberation mapping (Korista et al. 1995) and our estimated 80 ld inner edge of the dusty torus, we ran CLOUDY models corresponding to source distances of 7, 14, 21, 30, 50, and 80 ld. The continua at each of these radii were calculated as described above. Since there will certainly be a range of densities in the BLR, we ran models with hydrogen densities, n_H, of $10^{9.5}$, $10^{10.5}$, and $10^{11.5}$ cm^{-3}. Because they are located at the very centers of galaxies, the metalicities of AGNs are almost always supersolar (Hamann & Ferland 1999), so we adopted a metal abundance of three times solar. All models run were completely optically thick models and the calculations were continued far deeper into the clouds than any of the lines we are interested in were being produced.

In addition to these models we ran additional models to investigate the effect of not reducing the IR emission, and of varying the metal abundances from solar to six times solar. We also investigated the effect of significant (1000 km s^{-1}) (non-dissipative) internal turbulence (see Bottorff et al. 2000 and Bottorff & Ferland 2002).

10. BROAD-LINE COVERING FACTORS

In Table 4 we present the covering factors needed to produce the observed line fluxes. In order to show the effect of the radial distribution of the gas for each line we give the covering factors needed as a function of radius under the assumption that each line is only produced in gas at this radius. We show the effects of varying density, source distance, metal abundance, and continuum shape, and of adding turbulence. As well as giving covering factors using our standard continuum ("adopted") we also show the effects of using the simple linear interpolation across the EUV gap ("linear"), of using just the observed SED ("observed") with no corrections at all, and of not allowing for the BLR being far from the IR emission ("Extra IR"). As is to be expected, changing the EUV continuum shape has the biggest effect on the He II recombination lines (see, for example, Mathews & Ferland 1987). Adding extra IR heating increases the strengths of all collisionally-excited lines.

Looking at the density and radius dependencies of the covering factors for our standard model it can be seen that, as is well known (see, for example, Laor 2007), the production efficiency of most lines decreases at high ionizing flux levels. The efficiency generally increases with density for many lines except where lowering the resultant lowering of the ionization reduces the line flux (e.g., N V), or a line is collisionally suppressed (e.g., C III]).

The observed integrated line fluxes of an AGN are the sums of the contributions from all clouds at all densities and all radii (cf. the "LOC" model of Baldwin et al. 1995 and Korista & Goad 2000). In the bottom line of Table 4 we give the covering factors for an integrated model based on our standard continuum model, with a uniform range of densities from $10^{9.5}$ to $10^{11.5}$ cm^{-3}, and with uniform covering factor as a function of radius. There is generally good agreement in the resulting covering factors which range from 17–56% (ignoring He I λ5876 for which the observed flux is highly uncertain) and with an average is 40%. This average covering factor can be lowered somewhat by weighting the density distribution towards higher densities, and by having the covering factor increase with radius, but it can be seen from Table 4 that an average integrated covering factor of $< 20\%$ is not attainable. The only way of lowering the average covering factor to $< 20\%$ is by including substantial internal turbulence. Further lowering of the covering factor can be achieved by making the turbulence dissipative to provide additional heating for the low-ionization lines (Bottorff & Ferland 2002).

11. THE TORUS COVERING FACTOR

The dust covering factor, Ω_{dust}, can be found from the ratio of the bolometric luminosity, L_{bol}, to the luminosity, in the mid-infrared, L_{IR}. Since we have the complete spectrum for NGC 5548 we can perform a direct integration to obtain L_{Bol}. We show the results for different continuum assumptions in Table 5. The observed case ignores reddening and the host galaxy correction. The "low big bump" case is the simple linear interpolation across the EUV gap and the "high big bump" case is the more likely interpolation (see Fig. 6). The covering factors given in Table 5 assume that the torus has an unobstructed view of the higher-energy continuum. We will argue below that this is probably not the case.

12. VARIABILITY TRANSFER FUNCTIONS

The radial distribution of material in the BLR can only be inferred indirectly from reverberation mapping (see Peterson 2006 for a recent review). The most widely used measure of the size of the BLRs of AGNs is the "lag" given by the centroid of the cross-correlation function (Gaskell & Sparke 1986, Gaskell & Peterson 1987), but this has always been known to be biased towards gas at small radii. A better indication of the distribution of the gas is given by the transfer function $\Psi(\tau)$, which is the response of the system at a delay τ to a delta function at $\tau = 0$. A detailed comparison of observed and theoretical transfer functions is beyond the scope of this paper and will be given elsewhere, but in Figs. 7 – 9 we compare observed transfer functions of C IV and Hβ with simple theoretical transfer functions based on the parameters of our photoionization modelling.

Recovering the $\Psi(\tau)$ from observed continuum and line-flux time series is difficult. In addition to uncertainties arising from noise in the data (which are most significant for weak lines like those of He II), the derived $\Psi(\tau)$ depends on the sampling, the method used, and assumptions that always need to be made to recover $\Psi(\tau)$ in practice. Assumptions need to be made about the smoothness of $\Psi(\tau)$ and boundary conditions including the contribution of relatively non-varying components. It also needs to be recognized that some methods (e.g., the maximum-entropy method) only allow $\Psi(\tau)$ to be positive, so noise in $\Psi(\tau)$ gives spurious positive contributions at large delays. Since AGN variations are commonly quasi-cyclical on the timescale of almost all monitoring campaigns, aliasing at multiples of the quasi-period of the continuum variations will also make spurious contributions to $\Psi(\tau)$ at large delays. Because

TABLE 4
Covering Factors

Model	$\log(n_H)$	r(ld)	Lyα	N V	O I	λ1400	C IV	He II	C III]	Mg II	Hβ	He I
Adopted SED	9.5	7	74%	157%		192%	223%	25%	77%	212%	426%	
	9.5	14	28%	86%	417%	113%	131%	17%	32%	306%	80%	123%
	9.5	21	17%	60%	196%	85%	106%	19%	21%	119%	44%	66%
	9.5	30	13%	43%	135%	70%	83%	21%	16%	68%	28%	43%
	9.5	50	10%	28%	106%	54%	55%	22%	11%	28%	18%	29%
	9.5	80	9%	21%	87%	44%	35%	24%	10%	15%	15%	30%
	10.5	7	35%	43%	173%	77%	145%	15%	81%	526%	218%	181%
	10.5	14	19%	28%	36%	79%	101%	21%	60%	200%	97%	75%
	10.5	21	15%	22%	31%	64%	70%	22%	50%	101%	57%	50%
	10.5	30	13%	19%	34%	51%	48%	22%	46%	56%	39%	35%
	10.5	50	11%	24%	47%	37%	29%	24%	45%	23%	24%	22%
	10.5	80	10%	59%	48%	31%	24%	26%	44%	9%	17%	14%
	11.5	7	37%	20%	66%	91%	120%	26%	320%	290%	303%	159%
	11.5	14	27%	19%	50%	50%	60%	23%	364%	100%	128%	71%
	11.5	21	22%	27%	47%	35%	43%	22%	323%	50%	77%	42%
	11.5	30	20%	53%	49%	29%	39%	23%	278%	28%	50%	27%
	11.5	50	17%	256%	49%	29%	44%	24%	244%	12%	29%	15%
	11.5	80	15%		39%	49%	75%	26%	280%	6%	17%	10%
SED												
Observed	10.5	21	64%	55%	147%	69%	71%	100%	77%	51%	115%	107%
Adopted	10.5	21	15%	22%	31%	64%	70%	22%	50%	101%	57%	50%
Linear	10.5	21	22%	31%	38%	84%	74%	41%	75%	100%	65%	62%
Adopted	10.5	7	35%	43%	173%	77%	145%	15%	81%	526%	218%	181%
Extra IR	10.5	7	36%	32%	172%	55%	103%	17%	67%	437%	294%	206%
Fe/H												
Solar	10.5	7	36%	80%	723%	117%	139%	12%	104%	908%	207%	194%
3 solar	10.5	7	35%	43%	173%	77%	145%	15%	81%	526%	218%	181%
6 solar	10.5	7	36%	39%	92%	53%	135%	20%	68%	332%	225%	174%
3 solar	10.5	14	19%	28%	36%	79%	101%	21%	60%	200%	97%	75%
6 solar	10.5	14	21%	28%	23%	58%	108%	27%	49%	120%	97%	79%
Turbulence												
No turb.	10.5	7	35%	43%	173%	77%	145%	15%	81%	526%	218%	181%
Turb.	10.5	7	10%	25%	107%	37%	44%	17%	16%	33%	12%	21%
No Turb	10.5	21	15%	22%	31%	64%	70%	22%	50%	101%	57%	50%
Turb.	10.5	21	8%	16%	58%	20%	27%	21%	26%	12%	11%	25%
LOC Model			17%	34%	61%	51%	56%	22%	37%	28%	36%	13%

TABLE 5
ESTIMATED DUST COVERING FACTORS

Continuum Shape	Ω_{dust}
Observed (uncorrected)	61%
Internally de-reddened with low big bump	25%
Internally de-reddened with high big bump	19%

of these methodolical differences, a variety of different transfer functions have been published from the same data sets even for strong lines.

As is well known, $\Psi(\tau)$ for a thin spherical shell of radius r is a boxcar from $\tau = 0$ to $\tau = 2r/c$. The transfer functions for other spherically-symmetric distributions can be constructed by adding such boxcar functions. For example, a filled sphere has $\Psi(\tau)$ declining monotonically from a peak at $\tau = 0$. A hollow sphere of inner radius r_{in} has $\Psi(\tau)$ constant until $\tau = 2r_{in}/c$. If the clouds emit isotropically, the only way to avoid $\Psi(\tau)$ having a maximum at $\tau = 0$ is to have a non-spherical geometry. Most type-1 AGNs are observed close to pole on so we modelled non-spherically symmetric distributions as spheres with polar cones cut out of them viewed from on axis. A single thin sphere with a cap cut out around each of the poles gives $\Psi(\tau)$ as a box car of width $\pm \sin(\theta) r/c$ centered on r/c, where θ is the maximum angle the clouds subtended above the equatorial plane. $\Psi(\tau)$ for radially-thick distributions is simply the sum of these box cars. We calculated simple theoretical AGN line transfer functions, smoothed to the observed resolution, for clouds in a distribution which is truncated by cones on the symmetry axis, but is otherwise spherically symmetric. $\Psi(\tau)$ for geometries where the observer is slightly off axis, as will be the case for most AGNs, are mostly indistinguishable from on-axis cases. Off-axis cases can be divided into two classes: when the observer is inside the cone, and when he or she is outside the cone. If the opening of the cone is wide, the former case will be indistinguishable from the on-axis case, and if the opening of the cone is narrow, the latter case will be indistinguishable from spherical symmetry.

Our models have only three main parameters: the half-opening angle of the polar cone, $90\,\mathrm{deg} - \theta$, the outer radius, and the radial variation of responsivity which we parameterized as a simple power laws. The radial vari-

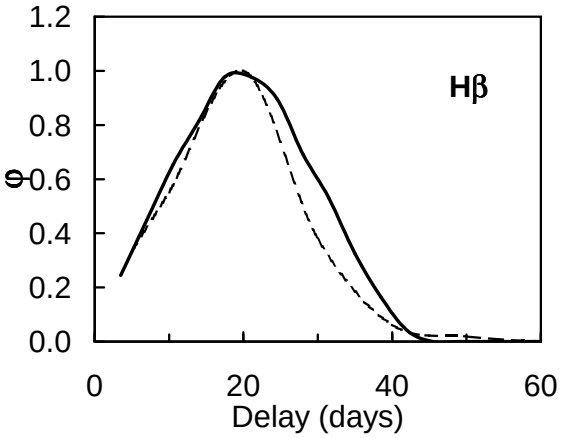

FIG. 7.— Theoretical (solid) and observed (dashed) transfer functions for Hβ in NGC 5548. The observed transfer function is from Horne, Welsh, & Peterson (1991).

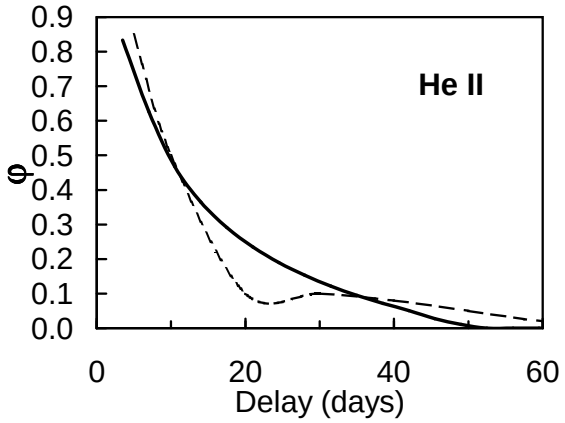

FIG. 8.— Theoretical (solid) and observed (dashed) transfer functions for He II λ1640 in NGC 5548. The observed transfer function is from Krolik et al. (1991).

ation of the responsivity depends on three things: the response of a particular line to changes in the ionizing continuum, the emissivity per cloud as a function of radius, and the dependence of the covering factor (number of clouds) as a function of radius. The functional form of the response of the flux in a given line from a cloud to changes in the continuum is expected to remain nearly constant over the range of conditions considered. The radial variation of responsivity thus depends on the change in emissivity, which is given by our photoionization models, and the unknown dependence of the covering factor on radius. For simplicity we assumed that the covering factor, which has to be the same for all lines coming from a given type of cloud, has no radial gradient, and that the radial variation in responsivity thus depends solely on the radial variation of emissivity given by the photoionization models. The remaining parameters for each transfer function are the opening angle and the outer radius. Although these assumptions are very simple, they nonetheless give useful insights into the behavior of transfer functions.

12.1. *The Hβ Transfer Function*

The photoionization models show that the emissivity of Hβ rises as $\sim r^{+1}$. Horne, Welsh, Peterson (1991) found that $\Psi(\tau)_{H\beta}$ (which we show as a dotted line in Fig. 7) does not peak at zero delay. Cacklett & Horne (2006) show that over the course of the 13-year IAW monitoring of NGC 5548 $\Psi(\tau)_{H\beta}$ maintained the same shape regardless of the mean flux level of NGC 5548. As outlined above, such a transfer function demands a predominantly non-spherical distribution[7] seen from within the polar opening. As can be seen in Fig. 7, we can readily reproduce the shape of $\Psi(\tau)_{H\beta}$ with our simple models. The symmetry of $\Psi(\tau)_{H\beta}$ requires $\theta \lesssim 25\,\mathrm{deg}$. This corresponds to a covering factor of 40% or less, and thus is in good agreement with the results in Table 4. For such a distribution, the position of the peak of $\Psi(\tau)$ depends only on the outer radius of the distribution. The outer edge of the BLR, r_{out} is expected to be the dust sublimation radius (Netzer & Laor 1993, Laor 2007) which is quite well defined. From consideration of IR reverberation mapping in section 2.2 we estimated that $r_{dust} \approx 80$ ld, but we can get a more precise estimate of r_{out} by fitting $\Psi(\tau)_{H\beta}$. At the optical flux level of NGC 5548 during the high state we are considering, Cackett & Horne (2006) find the peak of the $\Psi(\tau)_{H\beta}$ to be at 19 ld, with lower and upper quartile uncertainties of -2 and +5 ld respectively. This is consistent with the lag determined by the Korista et al. (1995). Fitting our model transfer function gives $r_{out} = 60$ ld with the same fractional uncertainty as in the position of the observed peak of $\Psi(\tau)_{H\beta}$.

12.2. *The He II Transfer Function*

The transfer function of He II was determined by Krolik et al. (1991). It is not as well determined as that of Hβ, but, as can be seen in Fig. 8, it shows a strong peak at zero delay. The emissivity of He II, unlike that of Hβ, declines slowly with radius as $\sim r^{-0.4}$. In our models this declining emissivity automatically gives $\Psi(\tau)$ peaking towards zero delay. The radical difference in the shape of $\Psi(\tau)_{H\beta}$ and $\Psi(\tau)_{HeII}$ thus primarily arises from photoionization physics (how clouds emit as a function of incident flux) rather than a profoundly different spatial distribution. Nonetheless, there must be some difference in the geometries of the clouds dominating the Hβ emission and those dominating the He II emission. If we are to keep the same flattened distribution derived from the $\Psi(\tau)_{H\beta}$ then $\Psi(\tau)_{HeII}$ declines too slowly with increasing delay. To make our model match the observed $\Psi(\tau)_{HeII}$ requires us to reduce r_{out} to ~ 30 days. However, if the clouds are directly exposed to the ionizing continuum (as in our CLOUDY models), we still have He II emission wherever there is Hβ emission, and the He II emitting cloud distribution would not be truncated more than the Hβ emitting cloud distribution. In this case another way of matching the shape of the He II transfer function (see Fig. 8) is to increase the covering factor. For pole-on viewing a covering factor of over 90% is needed ($\theta > 60\,\mathrm{deg}$). A more likely possibility is that the covering factor is only slightly greater than for Hβ (and hence in agreement with the results of Table 4), but we are now outside the hollow polar cone.

[7] Ferland et al. 1992 show how a spherical distribution can produce the Hβ transfer function if the emission is preferentially back towards the source, but this is unlikely since the Ly α transfer function in NGC 5548 is incompatible with such asymmetric emission. Also, the double-humped Hβ profile is independent evidence against spherical symmetry.

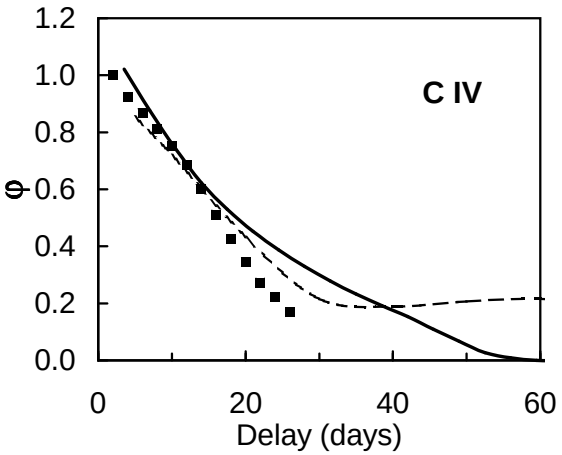

FIG. 9.— Theoretical and observed transfer functions for Hβ in NGC 5548. The theoretical transfer function (see text) is shown as a solid line. The squares are the transfer function derived with the SOLA method from the 1993 campaign (Wanders et al. 1995) and the dashed line is the transfer function derived from the 1989-90 campaign by Horne et al. (1991) using the maximum entropy method.

12.3. *The C IV Covering Factor*

In Fig. 9 we show $\Psi(\tau)_{CIV}$ estimated at two epochs by two different methods by Wanders et al. (1995) and Horne et al. (1991). Additional estimated C IV transfer functions can be found in these papers and also in Done & Krolik (1996). There is general agreement in $\Psi(\tau)_{CIV}$ for $\tau < 20$ d for both epochs, but more uncertainty for $\tau >$ 30 d. For C IV the radial dependence of the emissivity is intermediate between that of Hβ and He II. In the model shown in Fig. 9 we adopt a flat radial dependence. If we again assume $r_{out} \sim 60$d, as estimated from $\Psi(\tau)_{H\beta}$, then to fit the observed $\Psi(\tau)_{CIV}$ we need a high covering factor as for He II. Again this could really be a lower covering factor with us looking through the equatorial clouds. This is quite likely to be the case for NGC 5548 since the appearance of a double-humped, disk-like Hβ profile implies that we are not viewing it pole-on. It is also well known (see Arav et al. 2003, Steenbrugge et al. 2003 Steenbrugge et al. 2005, and refs. therein) that there is C IV absorption in NGC 5548.

13. DISCUSSION

13.1. *Is There an Energy-Budget Problem?*

We have considered in detail the overall SED of NGC 5548 during the high state at JD 2449120 and argue that although not all spectral regions were observed, we can be fairly confident of the overall SED. The main assumption still to be confirmed is the suggestion of Gaskell & Benker (2007) that the apparent turndown in the SED below Ly α is not intrinsic but results from a small amount of SMC-like dust. If this is incorrect, it only has a slight effect on our estimated covering factors.

The He II recombination lines, which are a very good indicator of covering factor since they are very insensitive to physical conditions, only require a covering factor of $\sim 25\%$ over a wide range of conditions with our adopted model. Other lines depend on physical conditions more but in our integrated ("LOC") model only two lines, O I λ1304 and C IV require covering factors of more than 50%. Only the He II flux depends significantly on our assumption that there is a small amount of SMC-like reddening. O I λ1304 is very sensitive to the metalicity and a slight increase in metalicity is sufficient to bring the O I covering factor in line with the other lines. High metalicity also lowers the covering factors needed for N V, the O IV] + Si IV λ1400 blend, and, to a lesser extent, C III]. Increasing the metalicity does not help reduce the C IV covering factor since it is a major coolant. What does help reduce the C IV covering factor most is an increased contribution of higher density gas. Higher density gas generally increases the emission efficiency of most lines.

From Table 4 it can be seen that with what we consider to be the best continuum, most of the lines can be explained by a covering factor of $\sim 40\%$ or somewhat less. This is not significantly lower than covering factors obtained in the past with weaker EUV continua (see, for example, Shields & Ferland 1993; Korista et al. 1998; Goad & Koratkar 1998; Kaspi & Netzer 1999; Korista & Goad 2000), so our main point is that even though we have argued that because of reddening there are more photons in the EUV continuum than hitherto recognized, *is it not possible to lower the covering factor significantly.* In particular, it is not possible to lower it to the level required by the Lyman limit absorption constraints. The reason why reddening does not solve the problem is that the lines have to be de-reddened as well as the continuum.

Independent support for the BLR covering factor we derive comes from the Fe Kα line equivalent width. Chiang et al. (2000) derive a Fe Kα covering factor of 20–25% for NGC 5548.

While all lines can be explained with covering factors significantly less than 100%, and so there is formally no "energy-budget" problem, we are unable to lower the necessary covering factors by an order of magnitude. In the old scenario of clouds uniformly covering the central source, a covering factor of $\sim 40\%$ (or even 20%) would still be a problem because Lyman continuum absorption is certainly not detected in 40% of AGNs. We believe that the solution to this problem, as proposed by Maiolino et al. (2001c), is that the clouds do *not* cover the source uniformly. Instead, they are in an axiumthally symmetric distribution and we are looking in through a hole at the pole. Important support for this comes from the line-continuum variability transfer functions discussed above. We have shown that the geometry implied by the well-measured Hβ transfer function is in good excellent quantitative agreement with this scenario. For other lines (e.g., C IV and He II) a less flattened distribution is needed. Additional support for a flattened geometry comes from the alignment of the polarization vector parallel to the axis of symmetry (see discussion in Goosmann & Gaskell 2007), and from polarization reverberation (Gaskell et al. 2007).

Since our deduced covering factors can be reconciled with line transfer functions for near pole-on viewing angles, we do not believe that there is an energy-budget problem for NGC 5548. This also makes some previously suggested solutions to the problem unnecessary. Given a flattened geometry there is no *need* for additional heating (Dumont et al. 1998) or for a large amount of turbulence (Bottorff et al. 2000, Bottorff & Ferland 2002) to reduce the covering factor, although such factors could still be relevant.

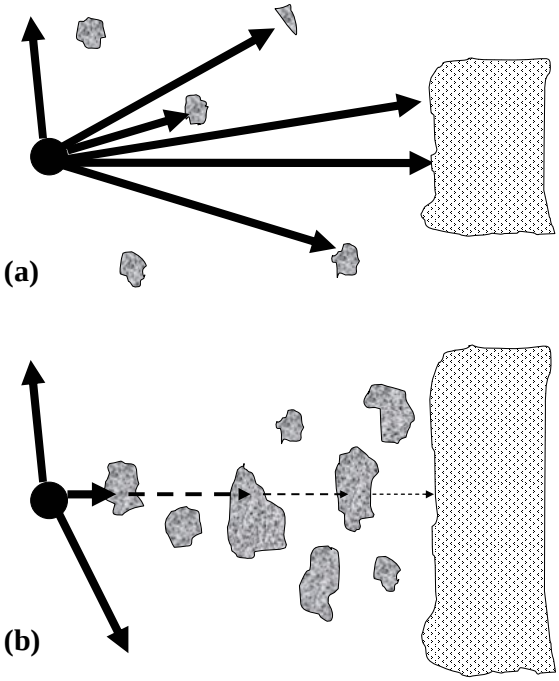

FIG. 10.— Schematic representation of BLR geometries. (a) Traditional model where BLR clouds are distributed quasi-spherically and mostly do not shield distant clouds or the torus. (b) Shielding model where the clouds are concentrated in the equatorial plane. The torus and distant clouds see the central source shielded by clouds closer to the center. (In both sketches the BLR clouds are not shown to scale and the number of clouds has been reduced by many orders of magnitude.)

TABLE 6
MEASURED AND PREDICTED LAGS FOR NGC 5548

Line		Observed[a]	LOC[b]	Shielded
Ly α	λ1216	12	8.5	12
N V	λ1240	4[c]	3.8	2.4
O I	λ1304	40[c]		43
Si IV + O IV]	λ1400	12	5.8	15
C IV	λ1549	8	8.0	8
He II	λ1640	3[d]	7.3[d]	3.3
C III]	λ1909	35	11.5	28
Mg II	λ2798	≥ 34	16	28
He II	λ4686	3[e]	7.3[d]	3.4
Hβ	λ4861	20[f]		18
He I	λ5876	13[g]		16
Hα	λ6563	22.5[g]		19

[a] From Clavel et al. (1991) except as noted.
[b] Based on Korista & Goad (2000) except as noted.
[c] From Krolik et al. (1991).
[d] From Bottorff et al. (2002).
[e] Set equal to λ1640 lag (see footnote 8).
[f] From Peterson et al. (1991).
[g] Scaled from Hβ using square of mean ratio of FWHMs from Osterbrock & Shuder (1982).

13.2. *A New BLR Model*

If the majority of the BLR gas is located within ± 25 deg of the equatorial plane, and the overall covering factor $\Omega/4\pi \approx 0.4$, then *photons leaving the central source in a direction close to the equatorial plane have a close to 100% probability of striking BLR gas.* By the time one gets to the inner edge of the dusty torus the spectrum has been substantially modified by passing through the inner BLR. Such modification of the spectrum has already been considered by Holt et al. (1980) and modelled for NGC 4151 by Ferland & Mushotzky (1982). The effect of shielding is similar to taking a standard cloud, cutting it in half in a plane perpendicular to the direction of the incoming photons and moving the outer part of the cloud further away. The BLR scenario we require resembles the geometry considered by MacAlpine (1972). In Fig. 10 we contrast our proposed shielded BLR geometry with the widely-used geometry where shielding is assumed to be negligible.

As discussed in 12.2 and 12.3, the differences in the transfer functions of C IV and Hβ require either that the high-ionization emission comes from a smaller region, or that it has a higher covering factor, or both. It has in fact long been argued that there are effectively two separate types of cloud: high-ionization clouds and low-ionization clouds (Gaskell 1987; Collin-Souffrin & Lasota 1988; Gaskell 2000). Not only are differences in radii implied by reverberation mapping, but the higher velocity dispersions of high-ionization lines (Osterbrock & Shuder 1982; Shuder 1982) show that the high-ionization gas is substantially closer (see Peterson & Wandel 1999). The blueshifting of high-ionization lines (Gaskell 1982) requires that the gas producing the high-ionization lines is spatially separated from the low-ionization gas. Furthermore, for NGC 5548 and other objects we find that the velocity dependence of physical conditions is different for the high- and low-ionization gas (Snedden & Gaskell 2004; Nazarova et al al. 2004, 2006; Snedden & Gaskell 2007a,b).

There have been attempts (notably by Korista & Goad 2000) to model this stratification in detail with a continuous distribution of cloud properties as in the LOC model, but there is a major difficulty in quantitatively matching the range of observed lags and line widths. As Korista & Goad (2000) point out, there are problems at both the high- and low-ionization ends: He II and N V have much *smaller* lags than predicted, while C III] and Mg II have significantly *longer* lags than predicted. He II presents another problem. The LOC models (Bottorff et al. 2002) predict that the radius of the He II emitting region should be only 10% smaller than the C IV emitting region, but as Bottorff et al. point out, the observations for NGC 5548 (in both 1989 and 1993), and for NGC 3783 (Reichert et al. 1994), Fairall 9 (Rodriguez-Pascual et al. 1997), NGC 7469 (Wanders et al. 1997), and 3C 390.3 (O'Brien et al. 1998) *all* give a lag of He II λ1640 three or four times smaller than the C IV lag.[8] In Table 6 we compare the observed lags for NGC 5548 (normalized to a C IV lag of 8 days) with the predictions of the LOC model predictions. The LOC predicted lags have also been scaled to a C IV lag of 8 days. It can be seen the LOC model only predicts a factor of four variation in lag while the observations give three times that.

The shielding model shown in Fig. 10b naturally ex-

[8] Bottorff et al. (2002) also point out a problem with He II λ4686 appearing to give a lag longer than that of He II λ1640. The explanation of the longer He II λ4686 delay is probably that a small amount of contamination by Fe II and the blue wing of Hβ makes the He II λ4686 lag appear longer. See Gaskell (2007).

plains the increased stratification. The relative order of ionization stages in a photoionized cloud is very insensitive to changes in the density or the ionizing flux; only the scale factor changes. We can therefore approximate a shielded distribution of clouds by taking a single cloud in CLOUDY and pretending that it has been broken into smaller pieces spread uniformly throughout the BLR. We simply linearly transform the depths into the cloud from the side facing the ionizing source into radii away from the central source. For different lines of sight and for different densities, cloud sizes, and filling factors the scale factor will be different, but the order of stages of ionization remains the same. The weighted mean radii of maximum emission of each line will therefore remain in the same ratios as the depths into a single cloud. One important difference from a single cloud is that photons can now escape from the distribution much more easily. We treated this in the same manner as dissipationless turbulence.

To quantitatively test the shielded BLR model, we took the 21 ld, $10^{10.5}$ cm^{-3} CLOUDY model with a 1000 km s^{-1} turbulence velocity, and scaled the radius of peak C IV emission to match the observed 8-day lag. The only other free parameter is the outer edge of the BLR which we took to be the 80 ld inner edge of the torus. We show our predicted lags in Table 6. As can be seen this give a better quantitative agreement with the observed lags (±20%) than the LOC model.

13.3. *The Torus Covering Factor*

Netzer & Laor (1993) proposed that the outer edge of the BLR is set by the dust-sublimation radius. Our modeling of transfer functions requires a fixed outer radius of ∼ 60d, and we have shown that this is in agreement with the radius of the hot dust measured by IR reverberation mapping.

We consider the most likely dust covering factor to be 19% (see section 11). This is lower than almost all the covering factors we deduced for the various emission lines in Table 4 and would imply that the dust has a flatter distribution than the gas.

The dust covering factor we find for NGC 5548 is similar to those of other AGNs. Maiolino et al. (2007) discuss the dust covering factors for a wide range of AGNs. They estimate the dust covering factor by assuming a ratio of $L_{Bol} = 7\nu L_\nu(\lambda 5200)$. However, the study of Shang et al. (2005) implies that $L_{Bol} = 15\nu L_\nu(\lambda 5200)$ is more appropriate, so that the covering factor can be calculated from

$$\Omega \approx 0.18\nu F_\nu(6.7\mu m)/F_\nu(5100\mathring{A}) \quad (6)$$

For NGC 5548 this gives $\Omega/4\pi \approx 0.18$ which is comparable to dust covering factors Maiolino et al. (2007) find for AGNs of comparable luminosity if we correct for our updated scaling of $\nu L_\nu(\lambda 5200)$ to L_{Bol}

Although the deduction of $\Omega_{dust}/4\pi \approx 0.2$ is straight forward and consistent with the covering factors we deduced for low-ionization lines, there is a problem: our NGC 5548 torus covering factor and similarly estimated covering factors for other AGNs are smaller than the torus covering factors implied by the observed ratio of type-1/type-2 AGNs. The ratio of type-1/type-2 AGNs in hard X-ray samples (see Fig. 7a of Maiolino et al. 2007) implies that at the luminosity of NGC 5548, $\Omega_{dust}/4\pi = 0.6$. A further problem of having $\Omega_{torus} < \Omega_{BLR}$ is that there should be many more objects where we see strong low-ionization absorption by the BLR (Maiolino et al. 2001c). While there are low-ionization broad absorption line AGNs, this absorption is not arising from the main BLR because it is blueshifted, and hence arising from outflowing gas. Because the variability of the blue wings of broad emission lines does not lead that of the red wings (Gaskell 1988; Koratkar & Gaskell 1989, Crenshaw & Blackwell 1990) the main BLR is not outflowing but is gravitationally bound. Observations indicate in fact that the BLR is *inflowing* slightly (Gaskell, 1988, Koratkar & Gaskell 1989, Koratkar & Gaskell 1991a,b, Korista et al. 1995; Done & Krolik 1995; Gaskell & Snedden 1997, Welsh et al. 2007). The problem of the lack of BLR absorption at the systemic velocity requires $\Omega_{torus} < \Omega_{BLR}$

We believe that our proposed BLR geometry offers the solution to these two problems: the BLR is almost certainly co-planar with the torus, so the latter does *not* have an unobscured view of the central source. Therefore, the energy received by the torus is substantially reduced, and hence the torus has to subtend a larger solid angle to explain the observed IR luminosity. If we assume that all of the energy from the Lyman limit to 1 keV is absorbed, the dust covering factor increases by a factor of 2.7 to 53%, which is consistent with the mean torus covering factor expected from the ratio of type-1/type-2 AGNs at the luminosity of NGC 5548.

13.4. *The Inner Radius of the Torus*

BLR absorption can also help another problem. Barvainis (1992) was able to satisfactorily explain the ∼ 400 d IR lag in Fairall 9 with dust sublimation temperatures of 1300 – 2000 K. However, Fairall 9 lies at the top of the IR lag-luminosity relationship shown in Fig. 1 and there is an order of magnitude scatter in the lag. NGC 5548 seems to lie close to the line in Fig. 1. Scaling the IR lag of Fairall 9 to NGC 5548 by $L^{1/2}$ would give a lag of ∼ 200 d. Since the grains are at ∼ 80 ld (or less), equation (3) of Barvainis (1987) shows that they would be at a temperature of ∼ 2500 K. This is too high for grain survival. In BLR shielding model, however, the continuum seen by the dusty torus in AGNs is absorbed by the BLR, and the dust grains can be much closer to the central source than they could otherwise be. For a factor of 2.7 reduction in the incident energy this allows the dust to be at ∼ 120 ld in NGC 5548. This is still greater than our estimated 80 ld. While this is within the observational uncertainties for NGC 5548, there are AGNs in Fig. 1 with substantially smaller dust lags for their luminosities, so an additional effect is needed. As Kishimoto et al. (2007) discuss, dust can survive closer to the central source if the dust grains are somewhat than those Barvainis (1987, 1992) considered. For larger dust grains the IR emissivity rises substantially (see Draine & Lee 1984) so they can cool much more efficiently and have lower equilibrium temperatures. There is good evidence from X-ray optical observations (Maiolino et al. 2001a,b) and optical-UV extinctions curves (Gaskell et al. 2005; Gaskell & Benker 2007) for dust grains in AGNs being larger than those in the local interstellar medium.

14. CONCLUSIONS

We have used simultaneous observations and the results of multi-wavelength variability studies to consider in detail the most probable SED of NGC 5548 during the highest state in the HST monitoring in 1993.

We have argued that when the continuum of NGC 5548 (and other AGNs) is corrected for Galactic and internal reddening, detailed photoionization modelling shows that the strengths of all the major emission lines can be explained by photoionization by the inferred AGN continuum so long as the covering factors are large ($\sim 40\%$). The long-standing "energy-budget problem" can now be seen to have been a consequence of not appreciating the significant reddening of the continua of most AGNs and erroneously assuming a spherical geometry. Because the emission-line strengths can be explained by photoionization from the observed (or extrapolated) continuum, there is no need for the additional heating source suggested by Collin-Souffrin (1986), Joly (1987), and Dumont et al. (1998).

To reconcile our high covering factor with the lack of absorption along the observer's line of sight we need a picture of the BLR which is different from the widely assumed quasi-spherical distribution of BLR clouds. Instead most of the BLR clouds (especially those far from the AGN) have a flattened distribution that extends out to the inner edge of the dusty torus. We have shown that such a model is consistent with the observed line-continuum transfer functions for NGC 5548.

In the geometry needed to explain the observed line strengths, the cloud covering fraction is close to 100% in the equatorial plane. We have therefore proposed a shielding model of the BLR where the inner clouds absorb much of the radiation before it reaches the outer clouds or the torus. This solves the problem of LOC models not explaining the strong change in cloud conditions with radius. The shielding BLR picture quantitatively reproduces the ionization-dependent lags seen in NGC 5548.

The absorption by BLR gas also solves several problems with the torus. Allowance for BLR absorption increases the torus covering factor calculated from energetics, and makes it slightly greater than the mean BLR covering factor. This reconciles the torus covering factor with the fraction of obscured (type-2) AGNs and explains why low-ionization by the BLR is never seen. The reduced flux seen by the torus also allows the dust to exist at smaller radii and reduces the discrepancy between the calculated dust sublimation radii and the radii of the inner edge of the torus found from reverberation mapping.

Since the line ratios, equivalent widths, and the continuum shape of NGC 5548 are similar to other AGNs (see, for example, Sergeev et al. 1999) we expect that these results can be generalized to most other AGNs.

We are grateful to Ski Antonucci for many fruitful discussions of reddening and torus covering factor issues. We are also grateful to Bruce Draine and Joe Weingartner for helpful discussions of dust issues, and to Bruce Draine for providing extinction models. We thank Phil Uttley for providing the RXTE X-ray light curve and Rebecca Harbison for assistance in collating optical photometry. This research has been supported by the Space Telescope Science Institute through grant AR-09926.01, and by the National Science Foundation through grant AST 03-07912.

REFERENCES

Arav, N., Kaastra, J., Steenbrugge, K., Brinkman, B., Edelson, R., Korista, K. T., & de Kool, M. 2003, ApJ, 590, 174
Abramowicz, M. A., Igumenshchev, I. V., & Lasota, J.-P. 1998, MNRAS, 293, 443
Barvainis, R. 1987, ApJ, 320, 537
Barvainis, R. 1992, ApJ, 400, 502
Binette, L., Fosbury, R. A., & Parker, D. 1993, PASP, 105, 1150
Binette, L., Magris C., G., Krongold, Y., Morisset, C., Haro-Corzo, S., de Diego, J. A., Mutschke, H., & Andersen, A. C. 2005, ApJ, 631, 661
Bohlin, R. C., Savage, B. D., & Drake, J. F. 1978, ApJ, 224, 132
Boller, T., Brandt, W. N., Fabian, A. C., & Fink, H. H. 1997, MNRAS, 289, 393
Boller, T., Brandt, W. N., & Fink, H. 1996, A&A, 305, 53
Bottorff, M., & Ferland, G. 2002, ApJ, 568, 581
Bottorff, M., Ferland, G., Baldwin, J., & Korista, K. 2000, ApJ, 542, 644
Bottorff, M. C., Baldwin, J. A., Ferland, G. J., Ferguson, J. W., & Korista, K. T. 2002, ApJ, 581, 932
Brotherton, M. S., Green, R. F., Kriss, G. A., Oegerle, W., Kaiser, M. E., Zheng, W., & Hutchings, J. B. 2002, ApJ, 565, 800
Cackett, E. M., & Horne, K. 2006, MNRAS, 365, 1180
Chiang, J., & Blaes, O. 2003, ApJ, 586, 97
Chiang, J., Reynolds, C. S., Blaes, O. M., Nowak, M. A., Murray, N., Madejski, G., Marshall, H. L., & Magdziarz, P. 2000, ApJ, 528, 292
Choloniewski, J. 1981, Acta Astron, 31, 293
Clavel, J., et al. 1992, ApJ, 393, 113
Collin-Souffrin, S. 1986, A&A, 166, 115
Collin-Souffrin, S., & Lasota, J.-P. 1988, PASP, 100, 1041
Congiu, E., Geminale, A., Barbaro, G., & Mazzei, P. 2005, J. Phys. Conf. Ser., 6, 161
Crenshaw, D. M., & Blackwell, J. H., Jr. 1990, ApJ, 358, L37
Crenshaw, D. M., & Kraemer, S. B. 2001, ApJ, 562, L29
Crenshaw, D. M., et al. 2002, ApJ, 566, 187
Czerny, B., Li, J., Loska, Z., & Szczerba, R. 2004, MNRAS, 348, L54
Davidson, K. 1972, ApJ, 171, 213
de Zotti, G., & Gaskell, C. M. 1985, A&A, 147, 1
Dietrich, M., et al. 2001, A&A, 371, 79
Done, C., & Krolik, J. H. 1996, ApJ, 463, 144
Done, C., Pounds, K. A., Nandra, K., & Fabian, A. C. 1995, MNRAS, 275, 417
Draine, B. T. 2003a, ApJ, 598, 1017
Draine, B. T. 2003a, ApJ, 598, 1026
Draine, B. T., & Lee, H. M. 1984, ApJ, 285, 89
Dumont, A.-M., Collin-Souffrin, S., & Nazarova, L. 1998, A&A, 331, 11
Edelson, R. A., & Malkan, M. A. 1987, ApJ, 323, 516
Ferland, G. J., Korista, K. T., Verner, D. A., Ferguson, J. W., Kingdon, J. B., & Verner, E. M. 1998, PASP, 110, 761
Ferland, G. J., & Mushotzky, R. F. 1982, ApJ, 262, 564
Ferland, G. J., Peterson, B. M., Horne, K., Welsh, W. F., & Nahar, S. N. 1992, ApJ, 387, 95
Gaskell, C. M. 1982, ApJ, 263, 79
Gaskell, C. M. 1987, in Astrophysical Jets and their Engines, ed. W. Kundt, (Dordrecht: Reidel), p. 29
Gaskell, C. M. 1988, ApJ, 325, 114
Gaskell, C. M. 2000, New Astronomy Review, 44, 563
Gaskell, C. M. 2007, in The Central Engine of Active Galactic Nuclei, ed. L. C. Ho and J.-M. Wang (San Francisco: Astron. Soc. Pacific), Vol. 373, p. 596
Gaskell, C. M. & Benker, A. J. 2007, ApJ, submitted [astro-ph/0711.1013]
Gaskell, C. M., Goosmann, R. W., Merkulova, N. I., Shakhovskoy, N. M., & Shoji, M. 2007, ApJ Letts., submitted [astro-ph/0711.1019]
Gaskell, C. M., & Klimek, E. S. 2003, Astron. Astrophys. Trans., 22, 661
Gaskell, C. M., & Peterson, B. M. 1987, ApJS, 65, 1
Gaskell, C. M., & Snedden, S. A. 1997, BAAS, 29, 1252
Gaskell, C. M., & Sparke, L. S. 1986, ApJ, 305, 175
Gierliński, M., & Done, C. 2004, MNRAS, 349, L7
Glass, I. S. 2004, MNRAS, 350, 1049
Goad, M., & Koratkar, A. 1998, ApJ, 495, 718

Goosmann, R. W., & Gaskell, C. M. 2007, A&A, 465, 129
Green, R. F., Pier, J. R., Schmidt, M., Estabrook, F. B., Lane, A. L., & Wahlquist, H. D. 1980, ApJ, 239, 483
Haba, Y., Kunieda, H., Misaki, K., Terashima, Y., Kaastra, J. S., Mewe, R., Fabian, A. C., & Iwasawa, K. 2003, ApJ, 599, 949
Hamann, F., & Ferland, G. 1999, ARA&A, 37, 487
Holt, S. S., Mushotzky, R. F., Boldt, E. A., Serlemitsos, P. J., Becker, R. H., Szymkowiak, A. E., & White, N. E. 1980, ApJ, 241, L13
Horne, K., Welsh, W. F., & Peterson, B. M. 1991, ApJ, 367, L5
Joly M., 1987, A&A, 184, 33
Kaastra, J. S., & Barr, P. 1989, A&A, 226, 59
Kaspi, S., & Netzer, H. 1999, ApJ, 524, 71
Kishimoto, M., Honig, S., Beckert, T., & Weigelt, 2007, A&Asubmitted
Kleinmann, D. E., & Low, F. J. 1970, ApJ, 159, L165
Koratkar, A. P., & Gaskell, C. M. 1989, ApJ, 345, 637
Koratkar, A. P., & Gaskell, C. M. 1991, ApJS, 75, 719
Koratkar, A. P., & Gaskell, C. M. 1991, ApJ, 375, 85
Korista, K. T., et al. 1995, ApJS, 97, 285
Korista, K., Ferland, G., & Baldwin, J. 1997, ApJ, 487, 555
Korista, K. T., Baldwin, J. A., & Ferland, G. J. 1998, ApJ, 507, 24
Korista, K. T., & Goad, M. R. 2000, ApJ, 536, 284
Laor, A., 477, 93
Laor, A., & Draine, B. T. 1993, ApJ, 402, 441
Laor, A. 2007, in "The Central Engine of Active Galactic Nuclei", ed. L. C. Ho and J.-M. Wang, ASP Conf. Ser. 373, 000 [astro-ph/0702577]
Li, A., & Draine, B. T. 2001, ApJ, 550, L213
Lyutyi, V. M., & Doroshenko, V. T. 1993, Astron. Lett., 19, 405
MacAlpine, G. M. 1972, ApJ, 175, 11
MacAlpine, G. M. 1981, ApJ, 251, 465
Magdziarz, P., Blaes, O. M., Zdziarski, A. A., Johnson, W. N., & Smith, D. A. 1998, MNRAS, 301, 179
Maiolino, R., Marconi, A., Salvati, M., Risaliti, G., Severgnini, P., Oliva, E., La Franca, F., & Vanzi, L. 2001a, A&A, 365, 28
Maiolino, R., Marconi, A., & Oliva, E. 2001a, A&A, 365, 37
Maiolino, R., Salvati, M., Marconi, A., & Antonucci, R. R. J. 2001c, A&A, 375, 25
Maiolino, R., Shemmer, O., Imanishi, M., Netzer, H., Oliva, E., Lutz, D., & Sturm, E. 2007, A&A, 468, 979
Markowitz, A., Edelson, R., & Vaughan, S. 2003, ApJ, 598, 935
Marshall, H. L., et al. 1997, ApJ, 479, 222
Marshall, H. L., Fruscione, A., & Carone, T. E. 1995, ApJ, 439, 90
Mathews, W. G., & Ferland, G. J. 1987, ApJ, 323, 456
McAlary, C. W., McLaren, R. A., & Crabtree, D. R. 1979, ApJ, 234, 471
McAlary, C. W., McLaren, R. A., McGonegal, R. J., & Maza, J. 1983, ApJS, 52, 341
McKee, C. F., & Petrosian, V. 1974, ApJ, 189, 17
Minezaki, T., Yoshii, Y., Aoki, T., Kobayashi, Y., Suganuma, M., Enya, K., Tomita, H., & Peterson, B. A. 2006, in AGN Variability from X-Rays to Radio Waves, ed. C. M. Gaskell, I. M. McHardy, B. M. Peterson and S. G. Sergeev, ASP Conf. Ser., 360, 79
Moshir, M., et al. 1990, BAAS, 22, 1325
Mould, J. R., et al. 2000, ApJ, 529, 786
Murphy, E. M., Lockman, F. J., Laor, A., & Elvis, M. 1996, ApJS, 105, 369
Nazarova, L. S., Bochkarev, N. G., & Gaskell, C. M. 2004, Astron. & Astrophys. Trans., 23, 343
Nazarova, L. S., Bochkarev, N. G., Gaskell, C. M., & Klimek, E. S. 2006, in AGN Variability from X-Rays to Radio Waves, ed. C. M. Gaskell, I. M. McHardy, B. M. Peterson and S. G. Sergeev, ASP Conf. Ser., 360, 255
Netzer, H. 1985, ApJ, 289, 451
Netzer, H., & Laor, A. 1993, ApJ, 404, L51
Neugebauer, G., Soifer, B. T., Matthews, K., & Elias, J. H. 1989, AJ, 97, 957
O'Brien, P. T., et al. 1998, ApJ, 509, 163
Oke, J. B. 1970, ApJ, 161, L17
Oke, J. B. 1974, ApJ, 189, L47
Oknyanskij, V. L., Lyuty, V. M., Taranova, O. G., & Shenavrin, V. I. 1999, Astron. Lett., 25, 483
Osmer, P. S. 1979, ApJ, 227,18
Osterbrock, D. E. 1977, ApJ, 215, 733
Osterbrock, D. E. 1989, Astrophysics of Gaseous Nebulae and Active Galactic Nuclei, (Mill Valley: University Science Books), p. 150
Osterbrock, D. E., & Shuder, J. M. 1982, ApJS, 49, 149
Papadakis, I. E., Petrucci, P. O., Maraschi, L., McHardy, I. M., Uttley, P., & Haardt, F. 2002, ApJ, 573, 92
Peterson, B. M. 2006, in AGN Variability from X-Rays to Radio Waves, ed. C. M. Gaskell, I. M. McHardy, B. M. Peterson and S. G. Sergeev, ASP Conf. Ser., 360, 191
Peterson, B. M., & Wandel, A. 1999, ApJ, 521, L95
Pounds, K. A., Reeves, J. N., Page, K. L., Edelson, R., Matt, G., & Perola, G. C. 2003, MNRAS, 341, 953
Preite-Martinez, A., & Pottasch, S. R. 1983, A&A, 126, 31
Pringle, J. E., & Rees, M. J. 1972, A&A, 21, 1
Reichert, G. A., et al. 1994, ApJ, 425, 582
Reimers, D., Hagen, H.-J., Schramm, J., Kriss, G. A., & Shull, J. M. 2005, A&A, 436, 465
Rieke, G. H. 1978, ApJ, 226, 550
Rieke, G. H., & Low, F. J. 1972, ApJ, 176, L95
Rodriguez-Pascual, P. M., et al. 1997, ApJS, 110, 9
Rokaki, E., Collin-Souffrin, S., & Magnan, C. 1993, A&A, 272, 8
Romanishin, W., et al. 1995, ApJ, 455, 516
Schlegel, D. J., Finkbeiner, D. P., & Davis, M. 1998, ApJ, 500, 525
Schmitt, H. R., Kinney, A. L., Calzetti, D., & Storchi Bergmann, T. 1997, AJ, 114, 592
Sergeev, S. G., Pronik, V. I., Sergeeva, E. A., & Malkov, Y. F. 1999, AJ, 118, 2658
Shakura, N. I., & Syunyaev, R. A. 1973, A&A, 24, 337
Shang, Z., et al. 2005, ApJ, 619, 41
Shapovalova, A. I., et al. 2004, A&A, 422, 925
Shields, G. A. 1973, Ph.D. Thesis, Caltech
Shields, G. A., Oke, J. B., & Sargent, W. L. W. 1972, ApJ, 176, 75
Shields, J. C., & Ferland, G. J. 1993, ApJ, 402, 425
Shuder, J. M. 1982, ApJ, 259, 48
Smith, M. G., et al. 1981, MNRAS, 195, 437
Snedden, S., & Gaskell, C. 2004, in AGN Physics with the Sloan Digital Sky Survey, ed. G. T. Richards & P. B. Hall, ASP Conf. Ser., 311, 197
Snedden, S. A. & Gaskell, C. M. 2007, 668, 000 [astro-ph/0403174]
Snedden, S. A. & Gaskell,C. M. 2007, submitted
Steenbrugge, K. C., Kaastra, J. S., de Vries, C. P., & Edelson, R. 2003, A&A, 402, 477
Suganuma, M., et al. 2004, ApJ, 612, L113
Suganuma, M., et al. 2006, ApJ, 639, 46
Stoy, R. H. 1933, MNRAS, 93, 588
Uttley, P., Edelson, R., McHardy, I. M., Peterson, B. M., & Markowitz, A. 2003, ApJ,584, L53
Walter, R., & Courvoisier, T. J.-L. 1990, A&A, 233, 40
Walter, R., Orr, A., Courvoisier, T. J.-L., Fink, H. H., Makino, F., Otani, C., & Wamsteker, W. 1994, A&A, 285, 119
Wanders, I., et al. 1997, ApJS, 113, 69
Wanders, I., & Peterson, B. M. 1996, ApJ, 466, 174
Welsh, W. F., Martino, D. L., Kawaguchi, G., & Kollatschny, W. 2007, to appear in The Central Engine of AGNs, ed. J.-M. Wang, ASP Conf. Ser. [astro-ph/0707.2606]
Weingartner, J. C., & Draine, B. T. 2001, ApJ, 548, 296
Winkler, H., Glass, I. S., van Wyk, F., Marang, F., Jones, J. H. S., Buckley, D. A. H., & Sekiguchi, K. 1992, MNRAS, 257, 659
Zanstra, H. 1931, Zeitschrift fur Astrophysik, 2, 1
Zheng, W., Kriss, G. A., Telfer, R. C., Grimes, J. P., & Davidsen, A. F. 1997, ApJ, 475, 469